PAPER • OPEN ACCESS

In situ probing of the thermal treatment of h-BN towards exfoliation

View the article online for updates and enhancements.

In situ probing of the thermal treatment of h-BN towards exfoliation

Zhengyu Yan[1]**, Amor Abdelkader**[2,*] **, Sarah Day**[3]**, Chiu Tang**[3]**,
Cinzia Casiraghi**[4] **and Wajira Mirihanage**[1,*]

[1] Department of Materials, The University of Manchester, Manchester M13 9PL, United Kingdom
[2] Faculty of Science and Technology, Bournemouth University, Poole BH12 5BB, United Kingdom
[3] Diamond Light Source, Harwell Science and Innovation Campus, Didcot OX11 0DE, United Kingdom
[4] Department of Chemistry, The University of Manchester, Manchester M13 9PL, United Kingdom

E-mail: wajira.mirihanage@manchester.ac.uk and aabdelkader@bournemouth.ac.uk

Abstract

Two-dimensional (2D) hexagonal boron nitride (h-BN) is becoming increasingly interesting for wider engineering applications. Thermal exfoliation is being suggested as a facile technology to produce large quantities of 2D h-BN. Further optimization of the process requires fundamental understanding of the exfoliation mechanism, which is hardly realized by *ex situ* techniques. In this study, *in situ* synchrotron x-ray powder diffraction experiments are conducted while heat treating bulk h-BN up to 1273 K. During the heating process, linear expansion of *c*-axis is observed and the contraction of *a*-axis up to around 750 K is consistent with previous research. However, a changing behavior from contraction to expansion in *a*-axis direction is newly observed when heating over 750 K. With the consideration of previous thermally oxidation studies, a hypothesis of thermal assisted exfoliation with oxygen interstitial and substitution of nitrogen at high temperature is proposed.

Supplementary material for this article is available online

Keywords: 2D material exfoliation, x-ray diffraction, hexagonal boron nitride

(Some figures may appear in colour only in the online journal)

Introduction

Since its discovery, graphene has attracted lot of attention due to its the outstanding electronic properties, such as high mobility and ballistic transport at room temperature, mechanical flexibility, transparency and high thermal conductivity, contrasting to bulk material [1–4]. Furthermore, the discovery of graphene started a new research field dedicated to two-dimensional (2D) materials: in nature there are many layered materials that can be exfoliated to single- and few-layers [5]. One of the most studied 2D material is hexagonal boron nitride (h-BN), which has the same honeycomb structure of graphene, but it is not identical as the carbon atoms are replaced by boron and nitrogen [6]. This gives rise to very different properties, compared to graphene, h-BN is a wide band gap material with high chemical and thermal stabilities and thermal conductivity [7–9]. This makes h-BN a good candidate for applications in 2D-based electronics, where it is used as encapsulation layer, dielectric and as substrate. Its smoothness and lack of dangling bonds allow to achieve the highest mobility in graphene-based devices, as compared to the SiO_2 substrate [10, 11]. 2D h-BN possesses strong resistance to oxidation at high temperature up to 1073 K, unlike graphene which goes for oxidation at temperatures above 700 K [12, 13]. Several researches have studied the thermal and mechanical properties of h-BN via first-principle calculation, a quantum mechanical simulation based on

density functional theory. Graphene and h-BN exhibit an unusual thermal contraction from 0 to 1500 K, while the single-layer transition-metal dichalcogenides (TMDC) materials, such as MoS_2 and $MoSe_2$, show a positive thermal expansion [14, 15]. 2D h-BN shows anisotropic mechanical properties that differ in armchair (parallel to B–N bond within a hexagon) and zigzag (perpendicular to B–N armchair) direction, and the B–N bonds tend to break along zigzag direction due to less ultimate strength [16].

The particular resistance to attack by molecular oxygen and most other gases opened the door for h-BN for applications such as flame retardant and a protective coating for high-temperature applications. Bulk h-BN, on the other hand, is less resistance to oxidation. In the presence of oxygen or hydroxyl ions, it transforms into boron nitride oxide or even boric acid. In fact, this phenomenon has been recently used to exfoliate a large amount of h-BN by Cui *et al* [12]. They observed a mass gain as oxygen incorporate into bulk h-BN lattice when heated in air at 1473 K. This material was transformed into hydroxylated boron nitride (BNO) upon stirring in water and exfoliated to h-BN nanosheet. Because of the oxygen functional groups on the surface, the produced BNO was able to form a stable dispersion in water, mimicking the surface properties of graphene oxide [12]. While the material was fully characterized, the exact mechanism of the exfoliation has not been investigated.

In this contribution, using *in situ* real-time XRPD, we are investigating the formation of in-plane thermal contraction that leads to structural distortion inside the h-BN lattice. The in-plane contraction is associated with expansion in the interlayer direction, which results in significant thermal effects concentrated between the layers. These thermal effects were also accompanied by decreasing in the crystallinity and weaken the van der Waal and lip–lip interaction between the layers, which facilitate the further exfoliation in water. Furthermore, the crystal after thermal treatment suffers from fast expansion upon reacting with water, which results in the exfoliation into hydroxylated 2D h-BN [17].

Experimental

The experiment was conducted at I11 Beamline of Diamond Light Source, UK. The heating cell was setup in the 2nd experimental hutch (EH2) equipped with a larger area detector and the synchrotron x-ray beam with 25 keV (monochromatic) was used for the diffraction measurements. The technical descriptions of the EH2 facility can be found in Murray *et al* [18]. Experimental h-BN samples were made by pressing (compacting) the powder into the disks (diameter 10 mm) with 2 mm thickness. The powder disk was placed within the customized hollow-shape electrical resistance furnace to carry out the heating and cooling cycles. The incident x-ray beam was parallel to the normal surface of the flat sample holding disk and the beam penetrated through the 2 mm thickness. The 2D Pixium area detector with 420×420 mm^2 (pixel size = 200 μm) was employed for

data collection. The detector was placed 1500 mm away from the sample.

The h-BN powder compacted samples with particle sizes 9 and 15 μm. The heating process is controlled by around 4 K min^{-1} up to 1263 K in the air, and then the furnace is left to cool down. Final diffracted intensity data is collected by integrating diffraction rings on the detector using DWAN® data analysis workbench prior to final processing with OriginPro®.

To complete the exfoliation, the thermally treated powder was washed with hot water and dried in an oven at 473 K for 4 h. The samples were then sonicated in distilled water for 30 min to form the stable suspension. After sonication and centrifugation, around 0.67 g of the exfoliated materials were collected from every 1 g on bulk h-BN.

Results and discussion

The XRPD pattern obtained at 400 K from two different h-BN particles with size of 9 and 15 μm are shown in figure 1(a). The *x*-axis is scattering vector (Q) which is calculated by $Q = (4\pi \sin \theta)/\lambda$. Where 2θ is the angle between incident and diffracted x-ray beams and λ is the wave length of the x-ray beam. Here, use of Q helps to generalize the different values in the diffraction angle (2θ), which varies with the wavelength of the used incident x-ray beam. The diffraction pattern of the first five peaks is studied to provide the established signature of h-BN. The result reflects the structure information in three lattice directions: (002) and (004) in the *c*-axis direction, (100) in *a*-axis direction, and (101) and (102) in a diagonal direction.

h-BN powder tends to arrange themselves with a basal plane parallel to the free surface of the sample, and this tendency is more significant for large particle size. As a result, (002) peak in figure 1(a) gives a very high diffraction intensity [19]. The x-ray diffraction data presents reciprocal space information, which is mathematically defined as the Fourier transform of the direct space details. In reciprocal space, the diffraction angle θ (scattering vector Q) is inversely related to the direct space, which means a smaller diffraction angle (which is related to the scattering vector) represents a larger distance in real space.

The h-BN consists of layers with hexagons of covalently bonded nitrogen (N) and boron (B) atoms, as shown in figure 1(b). The space group is P6$_3$/mmc, which is different from the closed packed hexagonal graphite (PG3/mmc), and the layers are directly stacked together with weak Van der Waals bonds. In particular, the Boron and Nitrogen atoms are alternatively arranged between the neighboring layers, directly on the other, while the carbon atoms in hexagonal structure are closed packed in the way of AB… For a hexagonal structure lattice, the Miller–Bravais indices composed of four numbers (*hkil*) is normally applied, which is established with the four Miller–Bravais vectors **a**$_1$, **a**$_2$, **a**$_3$ and **c** as shown in figure 1(b). The full indices transformation are given in table 1; where (00*l*) is the plane that perpendicular to **c** direction that provides the spacing of the different layers.
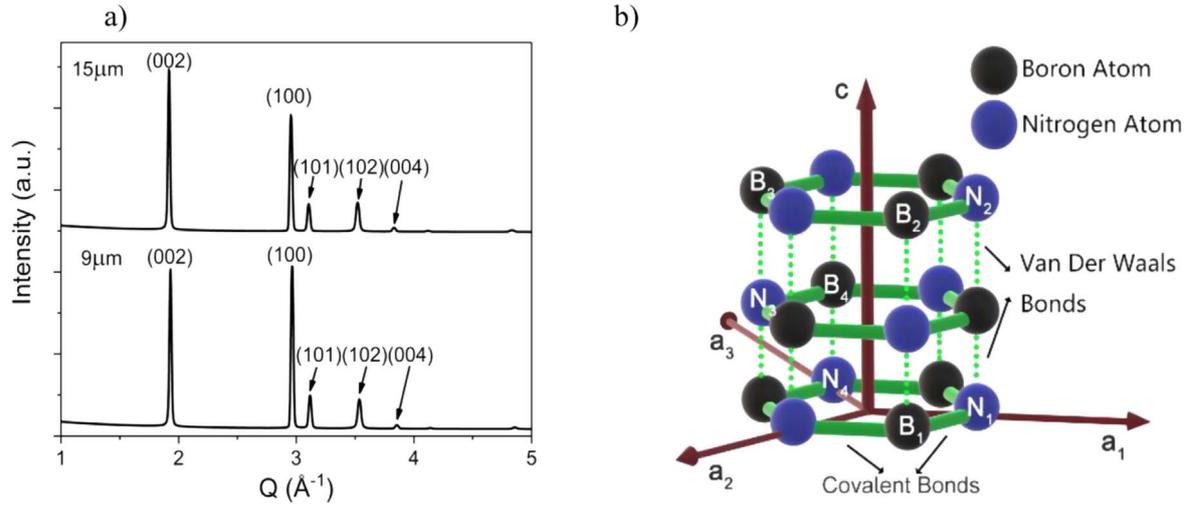
Figure 1. (a) Experimental x-ray powder diffraction pattern of h-BN particles at 400 K (particle size of 9 and 15 μm). The diffraction intensity is normalized with respect to (002) peak. (b) Schematic of hexagonal boron nitride (h-BN) structure. Boron (B) atom is shown in gray and nitrogen (N) atom in blue.

Table 1. Miller indices transformations and plane representation.

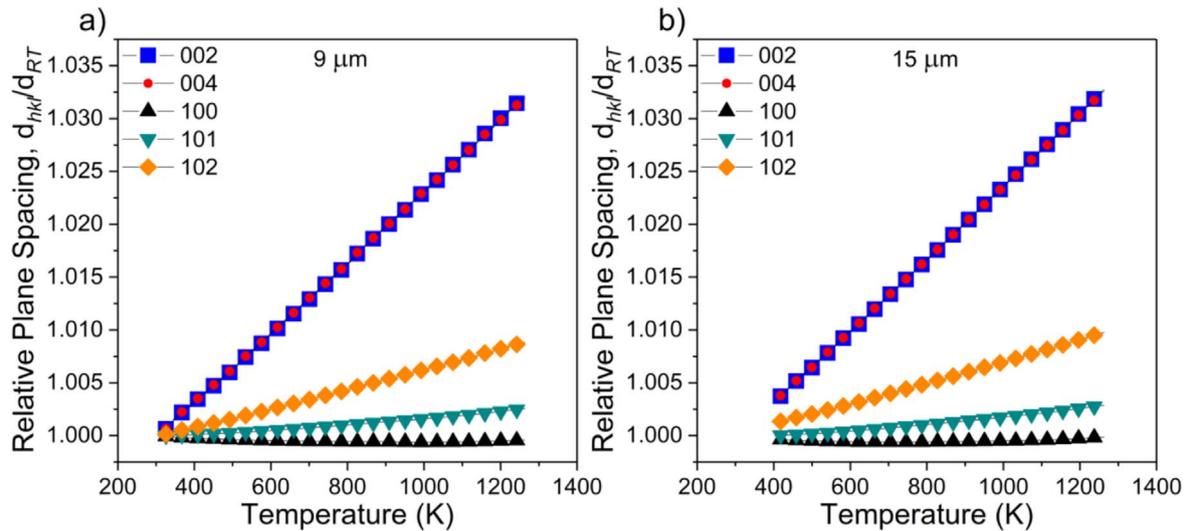| (hkl)	(0 0 2)	(1 0 0)	(1 0 1)	(1 0 2)	(0 0 4)
(hkil)	(0 0 0 2)	(1 0–1 0)	(1 0–1 1)	(1 0–1 2)	(0 0 0 4)
Plane	Basel	$B_1N_1B_2$	$B_1N_1B_3$	$B_1N_1N_3$	Basel

Figure 2. The relative plane spacing of h-BN (a) 9 μm *particle* and (b) 15 μm *particle* up to 1263 K. The relative plane spacing denotes the ratio of actual plane spacing (d_{hkl}) to the room temperature plane spacing (d_{RT}).

The calculated lattice parameters from the peak positions are $c = 6.525\,76 \pm 0.000\,005$ Å and $a = 2.455\,49 \pm 0.000\,005$ Å at room temperature, slightly less than that reported previously ($c = 6.658\,45$ Å and $a = 2.504\,05$ Å at room temperature) [6].

The relative plane spacing is defined as the ratio of the observed plane spacing to its value at room temperature (d_{hkl}/d_{RT}). As shown in figure 2, a general linear relation is obtained in the steady heating process. The (002) and (004) planes present the same expansion behavior which is reasonable as (002) and (004) are both (00*l*) planes expanding in

c-axis direction, hence the incremental proportion should be the same. Coefficient of thermal expansion of different planes (α_{hkl}) is defined by equation (1) as:

$$\alpha_{hkl} = \frac{1}{d_{RT}} \frac{\partial(d_{hkl})}{\partial T}, \tag{1}$$

where d_{RT} is (hkl) plane spacing at room temperature. This coefficient is equal to the linear gradient of the graphs in figure 2. The thermal expansion coefficient of (002) and (004) plane, α_{002} and α_{004}, give the largest thermal expansion of $\alpha_c = 34 \times 10^{-6}\,\text{K}^{-1}$ and it has a similar value for both
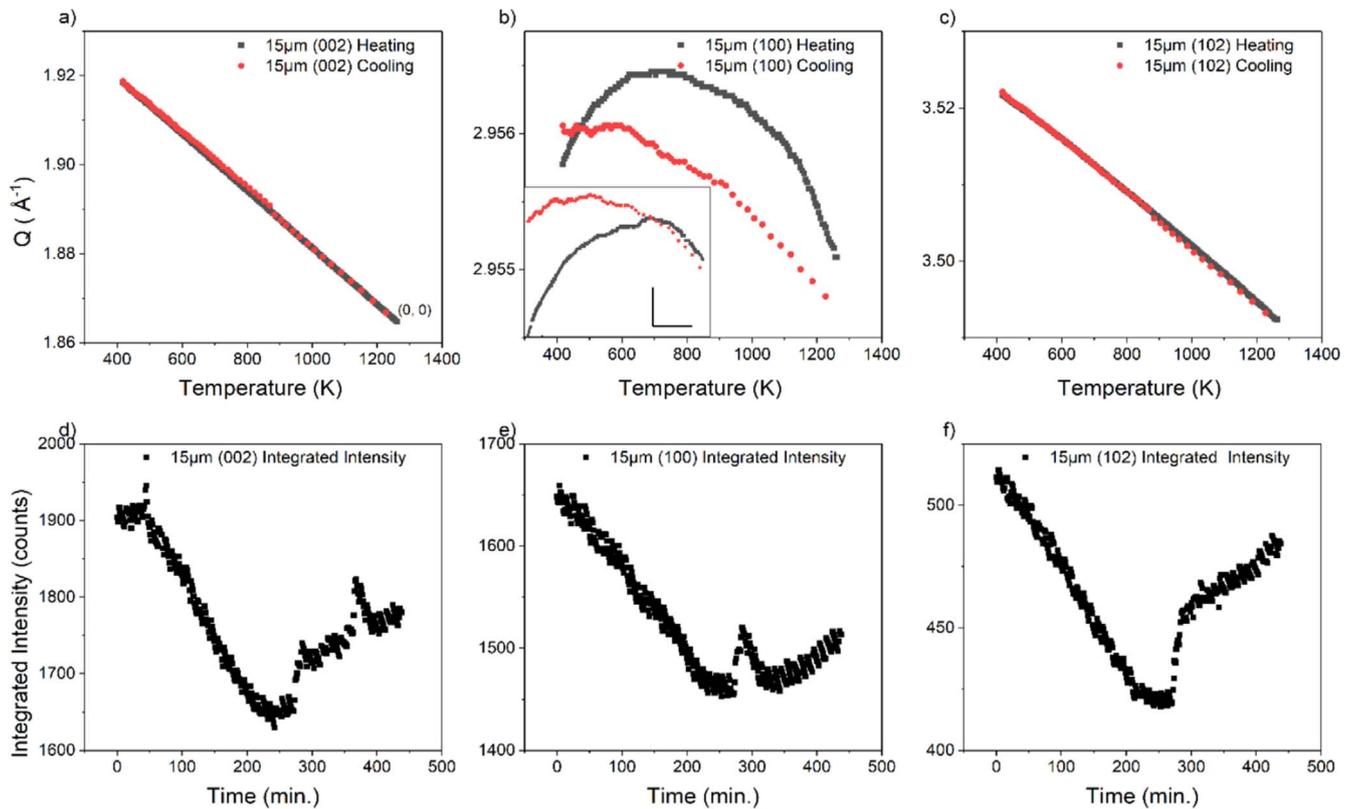
Figure 3. Experimental results of 15 μm sample: (a)–(c) are Q value during the heating and cooling process of (002), (100) and (102) planes; (d)–(f) are measured diffraction intensity versus experimental time of (002), (100) and (102) planes. The inset in (b) is 9 μm data with a turning point at about 950 K, with scale bar $T = 100$ K in x-axis and $Q = 0.0005$ in y-axis.

samples. Very small changes in the (100) plane are shown in figure 2 with an averaged negative thermal expansion coefficient, $\alpha_a = -0.35 \times 10^{-6}$ K^{-1}, which indicates plane (100) is not sensitive to the heating process. α_{101} and α_{102} are about 2.75×10^{-6} K^{-1} and 9.21×10^{-6} K^{-1}, respectively. They are much smaller than α_{002} but still shows expansion behavior. The results of $(h00)$ and $(00l)$ are smaller than previous research; $\alpha_a = -2.72 \times 10^{-6}$ K^{-1} and $\alpha_c = 37.7 \times 10^{-6}$ K^{-1} [20], $\alpha_a = -2.76 \times 10^{-6}$ K^{-1} and $\alpha_c = 38 \times 10^{-6}$ K^{-1} [21] and $\alpha_a = -2.9 \times 10^{-6}$ K^{-1} and $\alpha_c = 40.5 \times 10^{-6}$ K^{-1} [6].

The minor difference reported in this study compared with previous studies, which ranges up to 750 K, are most likely due to the thermal gradient between actual sample position and the set temperature of the furnace (which has the control thermocouple). However, a notable behavior is observed with *a*-axis results at higher experimental heating temperature from ~750 K up to 1273 K, where the behavior of (100) peak attributes changed from contraction to expansion. The (002) plane shows consistency with the thermal expansion results that the peak position of (002) moves linearly towards lower Q value (reciprocal space) as shown in figure 3(a), greater distance in real space. In the cooling process, the peak position linearly recovers to the original state (with x-axis from right to left). The (102) plane shows similar behavior with (002) plane.

The (100) interplane spacing changes ($|\Delta Q|$ spread ~0.0015 Å^{-1}) are small comparison with (002) plane ($|\Delta Q|$

spread ~0.06 Å^{-1}) as shown in figure 3(b). The (100) plane behaves contraction at start heating stage, and the plane changes to expansion at about 750 K (figure 3(b)). The h-BN expansion behavior has been experimentally studied from 10 to 297.5 K [20] and from 273 to 1073 K [6]. From 10 to 70 K, (100) plane expands slowly and changes to contraction from 70 K. Until near 973 K the contraction rate reduced to zero. In our experiment, the heating temperature is up to 1273 K, and a new turning point of (100) from contraction to expansion around 750 K is obtained as shown in figure 3(b). Although the turning point temperature of the 15 μm sample is below the converged contraction temperature of 973 K from previous research [6], this result indicates previously unreported expansion behavior along $\langle 100 \rangle$ at higher temperatures. This transition is similar to the transition around 70 K where it was considered as material specific property [20]. Further consideration of the such special material behaviors are beyond the scope of this manuscript while it is important highlight further physical understanding about such behavior through the *in situ* data presented here and previous work with similar *in situ* approach e.g. [6]. When considering the 9 μm sample presented in this study, it indicated a basic heating/cooling behavior similar to 15 μm sample while the turning point around 950 K is observed as shown in figure 3(b) (inset). In the cooling process of the 15 μm sample, (100) plane only shows contraction behavior with a reducing contraction rate, and final plane spacing recovers to a shorter distance than
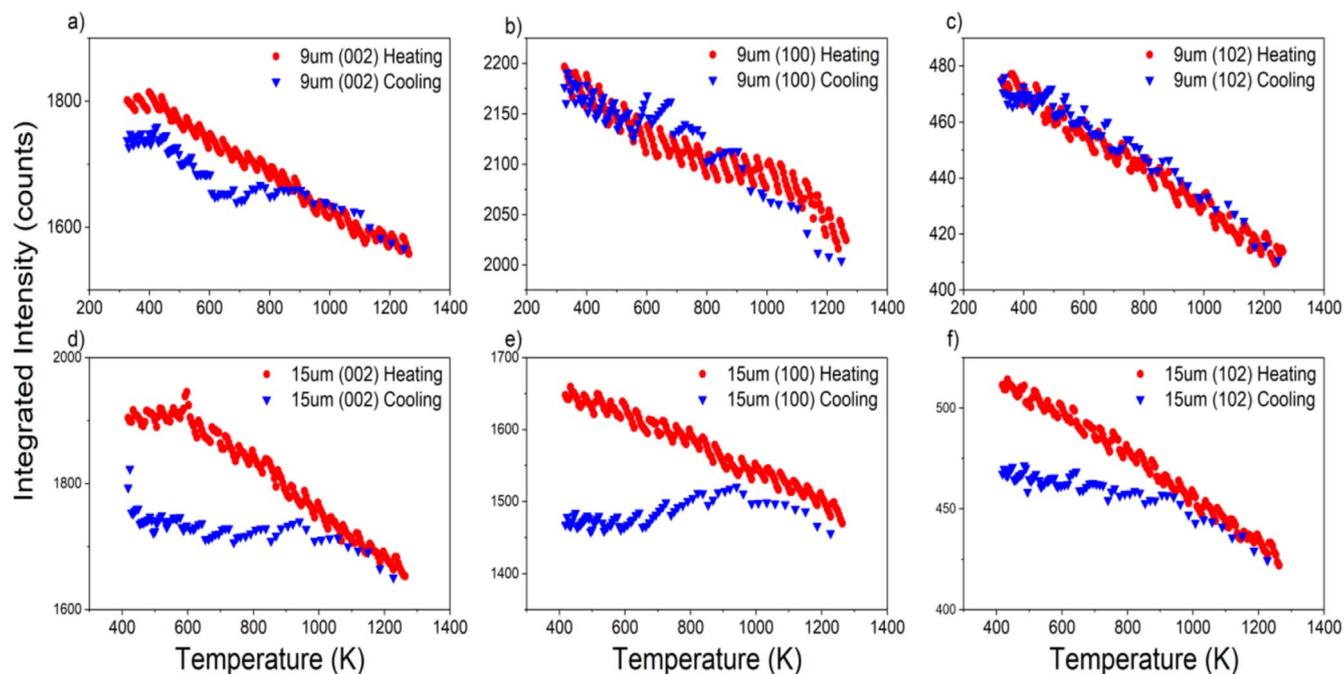
Figure 4. Experimental x-ray diffraction Intensity of (002) (100) and (102) planes of 9 and 15 μm h-BN. Scatters in red are heating process and scatters in blue are the cooling process.

initial spacing. Apart from that powder size do not indicate any significant different behaviors.

Figures 3(d)–(f) indicates peak intensity changes in this experiment. The intensity reduces with the heating process and then recovers while cooling. However, it is not possible to see the intensity is recovered to the initial intensity at room temperature level. These results suggested permanent distortion in the h-BN crystals. While cooling, the intensity increases fast at starting the cooling process, and increasing rate slows down as temperature decreases. There is an intensity 'jump' at about 380 min in (002) plane when temperature decreases to around 418 K, and after this point, the Q value of (002) plane becomes stable from an increasing process. Temperature decreases very slow after 418 K. Another intensity 'jump' at about 295 min in (002) and (100) plane can be seen, and this point is just below 1263 K when the cooling process starts.

Figure 4 presents the time evolved integrated XRPD peak intensity during the heating and cooling process, as a function of the temperature. As temperature increases, the intensity of the diffraction decreases due to the thermal motion of the atoms. The reduced intensity of the plane peaks while the thermal scattering intensity increases as shown in the diffraction background, which is called thermal diffuse scattering [22]. A nearly linear reduction of intensity is obtained for the heating process, but it is different during the cooling process. The intensity difference appears as the temperature cools down to the starting temperature, which is more significant in 15 μm samples. The intensity reduction of 15 μm (002) plane to the heating start intensity is about 7.8%, and that of (100) and (102) planes are about 10% and 8.25% respectively. The full-width of half-maximum of each peak is recovered to the same level after the cooling process (shown

in figure S1) (available online at stacks.iop.org/NANO/32/ 105704/mmedia), which means strain effect is not significant for the intensity difference. In this circumstance, the reduced intensity is most likely due to the exfoliation of h-BN mono-/ multi-layer flakes, the 2D h-BN. The reduced integrated intensity suggests a potential reduction of crystallinity, potentially a result of distortion-induced defects after the heating and cooling cycles. As reported in the literature, such defects in the layered structures facilitate the exfoliation by liquid phase methods [17, 23]. The 2D flakes start exfoliating from the top layer defect edges, such as the kink bands. Then, new defects can be generated on the following layers.

For the sample with 9 μm particle size, the peak intensity tends to recover during cooling and the difference between the initial and the final intensity is smaller than that of the 15 μm. At the end of the cooling process, the (002) intensity shows a tendency of decreasing which results in increasing intensity difference between heating and cooling process, however, (102) intensity recover to a similar level of the initial value. The intensity fluctuation of (100) may be caused by the layered structure disorder, as the covalent bond within the (00l) planes is much stronger than the Van der Waals bond between the (00l) planes. The rotation or translation can affect the order degree of (100) plane. In this case, the exfoliation would tend to take place in (00l) planes which is c-axis direction. The Van der Waals bonds partially break or weaken during the cooling. The particles are then easily exfoliated as a result of the weaker crystalline status in any subsequent step. In addition, the thermal treatment seems to cause more damage/distortion to the crystal structure with increasing the literal particles size (where high probability of having higher number of defects for bigger particle), as the exfoliation tends to start from the defects/dislocation. More

significant intensity difference is obtained for the large size particle.

When experimental configuration is concerned, the sample is placed in the middle of the furnace, in which case there may be a thermal gradient between the sample and the set point of the furnace. The difference could account for in the interpretation of thermal expansion data such as the lower rate(s) of expansion. The resolution of the instrument is not very high when using the area detector and 0.4×0.4 mm beam ($\Delta 2\theta \sim 0.015°$). Furthermore, the saw-tooth structure of intensity data, for example the cooling process in figure 4(b), is probably due to the top-up injection of the electron beam in the synchrotron ring machine that normally lasts 10 min. This will affect the x-ray beam intensity and the recorded data.

The intensity of (002) plane (in 9 μm sample) shows a flatten stage from 900 to 600 K in the cooling process and then increase with a higher rate, as shown in figure 4(a) (blue scatters). Then, a sudden intensity increase happens which may be related to the intensity 'jump' in figure 3(d) at about 380 K. This flatten stage is more pronounced for the 15 μm sample and takes place over wider temperatures range from 900 K to 400 K. Once the temperature decreased below 900 K, an obvious plateau of the intensity appears and continued until the end of the testing temperature for all peaks. This result is also consistent with the (100) plane expansion-contraction turning point and can be attributed to the in-plan oxygen doping of the h-BN sheet. The intensity difference in the (002) plan is most probably caused by the h-BN lattice distortion in the *c*-axis direction, which then facilitated the exfoliations in the subsequent step. Again, it is clear that the distortion is more pronounced in the powder with larger particles size.

The h-BN powder after the thermal treatment was readily dispersible in water after mild sonication for 30 min (supplementary figure S2). We have used several analysis techniques to characterize the produced materials, to ascertain 2D status of h-BN. Raman spectra of pristine h-BN and hydroxylated BN nanosheets from water suspensions show changes in integrated intensity and the position of peaks as shown in figure 5(a). It is reported that the multilayer h-BN shows downward shift with respect to bulk materials due to the induced strain [22, 24]. The AFM topographic image acquired by the tapping mode and the height profile confirmed that there are flakes with a thickness of about 1 nm and 1–2 μm lateral size shown in figure 5(b). The lateral size was further confirmed by the SEM imaging (supplementary figure S3). In some previous research, mainly based on the post process characterization methods, it has been suggested that heating h-BN in air produces an oxidizing phase with the boron atoms attached to three oxygen atoms in the extended crystal [12, 25]. Several other researchers suggest the hydrolyzation of h-BN upon cooling or during the subsequent washing in water. While the real-time measurement of the bulk h-BN did not show any significant phase changes, there are several pieces of evidence that might explain the mechanism of the exfoliation. The decrease in the unit cell in-plan parameters and the overall contraction of the unit cell in the

(100) plan after a heating-cooling cycle suggesting an irreversible process is taking place. The thermal effect induced stress due to the expansion-contraction cannot be responsible for the in-plan contraction since this kind of distortion is likely to cause expansion. Also, the thermal effect is likely to distort the out of plan direction because it is thermodynamically more favorable to break the weaker Van der Waal forces between the layers. The XPS wide scan evidences for presence of oxygen in the sampled after heating, and the high-resolution scan indications of a bond between boron and oxygen, is used to explain the change in the cell parameter [12]. However, interstitial oxygen cannot be responsible for the overall contraction in the (100) since all the interstitial atoms would rather cause expansion, as proposed by Cui etc [12]. The observation can be better explained through our results, proposing that oxygen replaces some of the nitrogen atoms; resulting in slightly shortens the distance between the in-plan atoms. This is also supported by the slight decrease in the Raman peak intensity as shown in figure 5(a), after the thermal expansion. The B-O bonding might be formed more easily at the defect edge, and this will accelerate the h-BN hydrolysis for sonication process. The 30 min 'milky' h-BN dispersion is quite similar to the dispersion that directly sonicated in water for 8 h [17].

In the first-principle modeling study of 2D h-BN [14], the linear thermal expansion coefficient (LTEC) of monolayer sheet is negative from 0 to 1500 K. The LTEC decreases sharply to from just below $0\,K^{-1}$ to $-7 \times 10^{-6}\,K^{-1}$ from 0 K to about 250 K, and then increase to $-2 \times 10^{-6}\,K^{-1}$ at 600 K. After 600 K, the LTEC increases with a decreasing rate and reaches at about $-0.7 \times 10^{-6}\,K^{-1}$ at 1500 K. This modeling gives a reference behavior of the (100) without the *c*-axis influence of the bulk material. The LTEC of monolayer h-BN remains negative from 0 to 1500 K and the difference between our (100) results, presumably caused by the 3D structure present in the samples used in the experiments. Another more specific explanation is related to oxygen replacement or interstitial. The heat treatment of h-BN under 1283 K for 60 min only obtained 5% weight gain [12], and the oxidation weight gain converged to about 17% after 350 min. Heating at the temperature of 1173 K did not show much oxidation, as about 7% weight gain after 500 min heating, and BN shows no oxidation weight gain below 1073 K. Our sample is maintained at 1273 K for 60 min, and no XRD peak for (010) of B(OH)$_3$ is observed [25]. Though the heating time over 1173 K is comparatively short, oxygen reaction should be involved. The interstitial of oxygen is a reasonable explanation of the in-plane expansion when heating up close to 1073 K, and most of these oxygen atoms escape as temperature cooling down. This is consistent with the temperature range of in-plane contraction-expansion changing. Finally, some of the oxygen remains as replacement of the nitrogen that results in the in-plane contraction with shorter B–O bonding.

The second factor that eased the exfoliation was the thermal-induced stress that has been introduced during the heating-cooling cycle by the uneven thermal expansion/contraction. The calculated thermal expansion coefficient in

the *c*-axis direction is way larger, reaching almost 300 times more than that for the in-plane direction. This uneven expansion leads to unequal distribution of stresses between the in-plan and interlayer direction, which triggers the formation of permanent thermal stresses. Since the in-plan bonds are partially ionic and therefore stronger, the induced thermal stresses are concentrated mainly between the layers. The lower crystallinity of the h-BN as evidenced by the lower peaks intensities also suggested the introduction of the reduction of the original structure breaking the bonds and/or distorting the original stable crystal structure. That can facilitate subsequent extensive exfoliation in water, once the h-BN is subjected to the heat treatment. The thermal effects weaken the van der Waals force between interlayers and the lip-lip interactions of h-BN, facilitating the exfoliation in the subsequent washing step. Zhu *et al* [26] have recently developed a method for the exfoliation of h-BN based on heating the bulk materials to 1073 K followed by quenching in liquid nitrogen and proposed that the fatigue produced by the expansion-contraction was partially responsible for the exfoliation. Hence, the real-time measurement of the thermal expansion coefficient gives clear evidence on the role of uneven expansion and the role of thermal stresses on the exfoliation. Further, it needs to point out that the absence of oxygen or presence of any other specific gaseous environment triggers such mechanisms differently. Therefore, apart from current results which show the promise *in situ* PXRD studies, it warranted the requirement of further *in situ* studies in obtaining extended understanding about the dynamic structure changes while the heat treatment of h-BN. Particularly studies under specific gaseous environments will facilitate to establish the conclusive details of the potential nitrogen–oxygen interchanged mechanism with h-BN at high temperatures.

Conclusions

In this paper, we present the real-time x-ray diffraction measurements taking the thermal treatment of h-BN towards the exfoliation into the 2D allotrope. The layered structure exhibits linear expansion, as shown in figure 3(a) during the heating process in *c*-axis direction as expected. However, in the *a*-axis direction figure 3(b), within basal plane, it shows contraction behavior up to 750 K in the beginning of the heating process, and changes from contraction to expansion gradually as temperature heating above 750 K. At almost the same temperature, a changing behavior has been observed in the diffraction intensity during the cooling process that a 'flatten stage' obtained. This coincidence of the peak position and intensity is related to the exfoliation mechanism. The heat-treated powder was readily exfoliated after 30 min of sonication, leading to the formation of 2D h-BN dispersion in water. According to previous thermal exfoliation research of h-BN, the oxidization is normally included. However, the XRPD peaks profile did not show obvious new peaks or changes for oxidation. This work benchmarks the potential for *in situ* x-ray studies to reveal exfoliation mechanisms, it

indicates the necessity of further extensive experimental work to obtain complete understanding of the dynamic process involve with exfoliation of 2D materials.

Author contributions

AA and WM conceived the approach and designed the experiments. AM, WM, SD and CT carried out the experiments. ZY analysis the data and draft the manuscript with inputs from CC, WM and AA. All authors discussed the results and commented on the manuscript.

ORCID iDs

Amor Abdelkader ⬤ https://orcid.org/0000-0002-8103-2420
Cinzia Casiraghi ⬤ https://orcid.org/0000-0001-7185-0377
Wajira Mirihanage ⬤ https://orcid.org/0000-0002-9083-269X

References

[1] Novoselov K S 2004 Electric field effect in atomically thin carbon films *Science* **306** 666–9
[2] Geim A K and Novoselov K S 2007 The rise of graphene *Nat. Mater.* **6** 183–91
[3] Kusmartsev F V, Wu W M, Pierpoint M P and Yung K C 2014 *Application of Graphene Within Optoelectronic Devices and Transistors* (Singapore: Springer) arXiv:1406.0809 [Cond-Mat]
[4] Balandin A A, Ghosh S, Bao W, Calizo I, Teweldebrhan D, Miao F and Lau C N 2008 Superior thermal conductivity of single-layer graphene *Nano Lett.* **8** 902–7
[5] Nicolosi V, Chhowalla M, Kanatzidis M G, Strano M S and Coleman J N 2013 Liquid exfoliation of layered materials *Science* **340** 1226419
[6] Pease R S 1952 An x-ray study of boron nitride *Acta Crystallogr.* **5** 356–61
[7] Chen Y, Zou J, Campbell S J and Le Caer G 2004 Boron nitride nanotubes: pronounced resistance to oxidation *Appl. Phys. Lett.* **84** 2430–2
[8] Sichel E K, Miller R E, Abrahams M S and Buiocchi C J 1976 Heat capacity and thermal conductivity of hexagonal pyrolytic boron nitride *Phys. Rev.* B **13** 4607–11
[9] Cai Q, Scullion D, Gan W, Falin A, Zhang S, Watanabe K, Taniguchi T, Chen Y, Santos E J G and Li L H 2019 High thermal conductivity of high-quality monolayer boron nitride and its thermal expansion *Sci. Adv.* **5** eaav0129
[10] Withers F *et al* 2014 Heterostructures produced from nanosheet-based inks *Nano Lett.* **14** 3987–92
[11] Dean C R *et al* 2010 Boron nitride substrates for high-quality graphene electronics *Nat. Nanotechnol.* **5** 722–6

[12] Cui Z, Oyer A J, Glover A J, Schniepp H C and Adamson D H 2014 Large scale thermal exfoliation and functionalization of boron nitride *Small* **10** 2352–5

[13] Liu L, Ryu S, Tomasik M R, Stolyarova E, Jung N, Hybertsen M S, Steigerwald M L, Brus L E and Flynn G W 2008 Graphene oxidation: thickness-dependent etching and strong chemical doping *Nano Lett.* **8** 1965–70

[14] Sevik C 2014 Assessment on lattice thermal properties of two-dimensional honeycomb structures: graphene, h -BN, h -MoS$_2$, and h -MoSe$_2$ *Phys. Rev.* B **89** 035422

[15] Çakır D, Peeters F M and Sevik C 2014 Mechanical and thermal properties of h -MX$_2$ (M = Cr, Mo, W; X = O, S, Se, Te) monolayers: a comparative study *Appl. Phys. Lett.* **104** 203110

[16] Peng Q, Ji W and De S 2012 Mechanical properties of the hexagonal boron nitride monolayer: *ab initio* study *Comput. Mater. Sci.* **56** 11–7

[17] Lin Y, Williams T V, Xu T-B, Cao W, Elsayed-Ali H E and Connell J W 2011 Aqueous dispersions of few-layered and monolayered hexagonal boron nitride nanosheets from sonication-assisted hydrolysis: critical role of water *J. Phys. Chem.* C **115** 2679–85

[18] Murray C A, Potter J, Day S J, Baker A R, Thompson S P, Kelly J, Morris C G, Yang S and Tang C C 2017 New synchrotron powder diffraction facility for long-duration experiments *J. Appl. Crystallogr.* **50** 172–83

[19] Thomas J, Weston N E and O'Connor T E 1962 Turbostratic boron nitride, thermal transformation to ordered-layer-lattice boron nitride *J. Am. Chem. Soc.* **84** 4619–22

[20] Paszkowicz W, Pelka J B, Knapp M, Szyszko T and Podsiadlo S 2002 Lattice parameters and anisotropic thermal expansion of hexagonal boron nitride in the 10 ∼ 297.5 K temperature range *Appl. Phys. Mater. Sci. Process.* **75** 431–5

[21] Yates B, Overy M J and Pirgon O 1975 The anisotropic thermal expansion of boron nitride: I. Experimental results and their analysis *Phil. Mag.* **32** 847–57

[22] Gorbachev R V *et al* 2011 Hunting for monolayer boron nitride: optical and Raman signatures *Small* **7** 465–8

[23] Li Z *et al* 2020 Mechanisms of liquid-phase exfoliation for the production of graphene *ACS Nano* **14** 10976–85

[24] Abdelkader A M and Kinloch I A 2016 Mechanochemical exfoliation of 2D crystals in deep eutectic solvents *ACS Sustain. Chem. Eng.* **4** 4465–72

[25] Yu B, Xing W, Guo W, Qiu S, Wang X, Lo S and Hu Y 2016 Thermal exfoliation of hexagonal boron nitride for effective enhancements on thermal stability, flame retardancy and smoke suppression of epoxy resin nanocomposites via sol–gel process *J. Mater. Chem.* A **4** 7330–40

[26] Zhu W, Gao X, Li Q, Li H, Chao Y, Li M, Mahurin S M, Li H, Zhu H and Dai S 2016 Controlled gas exfoliation of boron nitride into few-layered nanosheets *Angew. Chem., Int. Ed.* **55** 10766–70